INTERNATIONAL JOURNAL OF PRECISION ENGINEERING AND MANUFACTURING Vol. 19, No. 1, pp. 13-22 JANUARY 2018 / 13

REGULAR PAPER

DOI: 10.1007/s12541-018-0002-6
ISSN 2234-7593 (Print) / 2005-4602 (Online)

Damping Controller Design for Nanopositioners: A Hybrid Reference Model Matching and Virtual Reference Feedback Tuning Approach

Jie Ling[1], Zhao Feng[1], Min Ming[1], and Xiaohui Xiao[1,#]

1 School of Power and Mechanical Engineering, Wuhan University, No. 8, South Donghu Road, Wuchang District, Wuhan, 430072, China
Corresponding Author / E-mail: xhxiao@whu.edu.cn, TEL: +86-13720360269

KEYWORDS: Damping control, Reference model matching, Virtual reference feedback tuning, Piezo-actuated nanopositioner, Tracking control

Conventionally, fixed-structure feedback controllers are designed by model-based approaches. However, such controllers are not necessarily ideal and optimal when connecting with the actual plant because of the existence of modeling uncertainty. In this paper, a paralleled damping controller as well as a novel hybrid reference model matching (RMM) and virtual reference feedback tuning (VRFT) approach for parameters' tuning of the controller is presented. The composite damping controller for piezo-actuated nanopositioners is fixed-structure and low-order that uses a high-gain notch filter and a high-pass resonant controller to damp the first resonant peak. The proposed hybrid tuning approach combines an identified system model and a set of experimental input/output data into the parameters' optimization of the proposed composite damping controller. The proposed hybrid approach simplifies the tuning process by decreasing the number of the parameters in the initial values' choosing stage from the whole nine to four. Besides, the application of experimental data improves rejection of model uncertainty. A set of optimal parameters in the controller is obtained using the proposed hybrid design approach. Experimental results with comparisons to built-in PID controller are presented to show the effectiveness of the composite damping controller optimized via the hybrid approach.

Manuscript received: January 2, 2016 / Revised: March 11, 2017 / Accepted: August 15, 2017

NOMENCLATURE

VRFT = Virtual Reference Feedback Tuning
RMM = Reference Model Matching
RC = Resonant Control
IRC = Integral Resonant Control
SISO = Single-Input Single-Output
MIMO = Multi-Input Multi-Output

1. Introduction

Nanopositioners are widely used to achieve fine mechanical displacements in applications such as atomic force microscopy,[1] nanometrology,[2] high-density data storage system,[3] semiconductor device manufacturing,[4] fiber optic alignment,[5] chemical science and engineering,[6] etc. To be more special, for systems such as video-rate scanning probe microscopies,[7] the motion reference trajectories repeat from one period to the next and the motion should be as fast and accurate as possible to study fast dynamic processes like the movement of biological cells in real time.[8,9] Piezo-stack-actuated flexure nanopositioning stages are ideal for high-speed high-resolution positioning as the pizeo-actuators can provide large forces and friction-less motion.[10] For image scanning of speciments, the nanopositioners are commonly actuated in a taster pattern with a triangular signal in the X-axis.[11] The triangular signal contains all odd harmonics of its basic frequency, which can excite the first mechanical resonance mode of the nanopositioner.[12] So the positioning accuracy of high-speed nanopositioners is limited mainly due to vibrations caused by this excited mechanical resonance.[1,11-14]

Research works to achieve high-speed high performance nanopositioning focus on both flexure-based mechanism and control system design.[1,14] Many special mechanical structures have been designed and optimized to ensure the highest possible mechanical

resonance.[15-17] However, with the existence of unexpected vibration caused by excitation of the resonant modes, the raster scanning speed of piezo-actuated nanopositioners is often limited to about 1% of the first mechanical resonance frequency.[18] Herein, the focus in this paper is the damping control strategies for vibration rejection.

The damping controllers designed for nanopositioners can be divided into two categories: 1) feedforward control[19-21] and 2) feedback control.[22-28] Feedforward controllers like system dynamics inversion,[19] iterative learning control[20] and input shaping[21] can provide very good results. However, feedback controllers are still necessary to reduce sensitivity to uncertainty and external disturbance.[10,22] General model-based control laws can also be used in feedback damping controller design, such as H_∞ control,[23] loop-shaping approach,[24] linear matrix inequalities based control[25] and so on. Besides, the fixed-structure low-order feedback control laws are practical for the ease of implementation and low computational complexity. These controllers include positive position feedback,[26] polynomial-based pole placement,[27] positive velocity and position feedback,[28] resonant control (RC) for single-input single-output (SISO) systems,[29,30] and for multi-input multi-output (MIMO) systems, and integral resonant control (IRC),[31-33] high-gain notch filter.[34] However, most aforementioned feedback damping controller[26-34] are designed through model-based approach, i.e., a mathematical model of the plant is identified and used to compute the fixed-order controller. This controller is not necessarily ideal and optimal when connected to the plant, and the control performance is weakened by modeling uncertainty.[35]

Some data-driven approaches have been proposed to design reliable fixed-structure feedback controllers off-line with a limited number of open-loop or closed-loop experiments. The plant modeling work can be skipped, by directly tuning the controller parameters with data collections.[36] These approaches include self-tuning regulation,[37] iterative feedback tuning (IFT),[38] iterative correlation-based tuning (ICbT),[39] virtual reference feedback tuning (VRFT)[40] and so on. The IFT method minimizes a quadratic cost using several closed-loop experiments iteratively and needs at least three sets of experimental data. The ICbT method minimizes the crosscorrelation function between the closed-loop output error and the reference signal iteratively. While, the VRFT approach is a non-iterative and one-shot optimization method, which uses the open-loop experimental data instead of the closed-loop data. However, unlike the model-based case, few works concerning damping controller design using a data-driven technique like the VRFT approach have been studied.

The motivation of this paper is to design a damping controller for a pizeo-actuated nanopositioner using the data-driven VRFT approach instead of conventional model-based approach. A low-order notch filter was applied to modify the sharp resonant peak of the open-loop system to reject vibration as demonstrated by Kam et al.[34] However, the bandwidth of the closed-loop control system with a feedback notch filter was not ideal. An IRC paralleled with a high-pass RC was designed to reject vibration and increase the closed-loop bandwidth at the same time.[13] In this paper, a high-gain notch filter paralleled with a high-pass resonant controller was adopted. Then, the reference model matching (RMM) approach was applied to determine the parameters in the denominator of the controller, while the data-driven VRFT approach was adopted to calculate the optimal parameters in the numerator of the

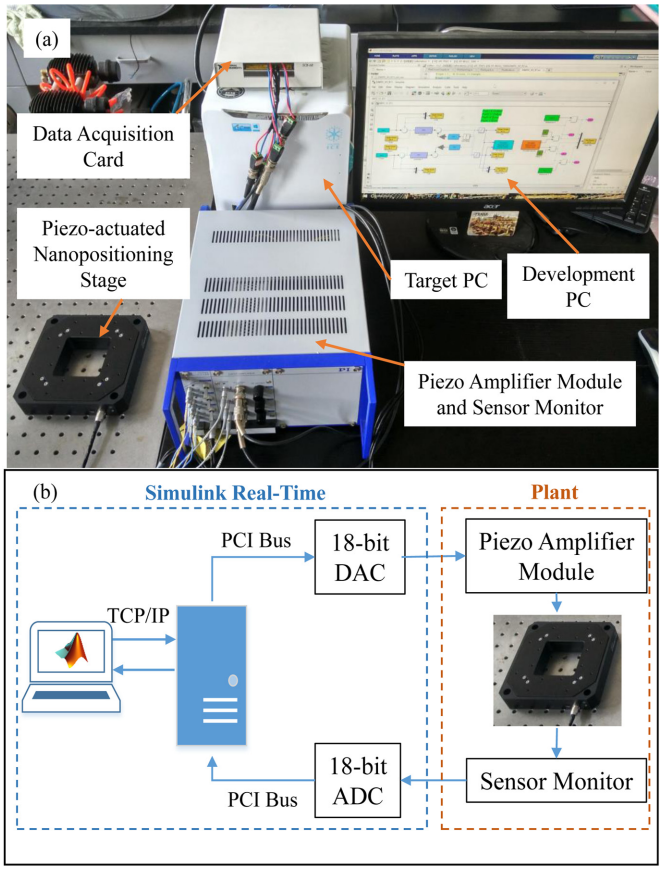

Fig. 1 The experimental setup of the piezo-actuated nanopositioning stage (a) Experimental platform (b) Block diagram of the signal flow

controller using one-shot experimental data. The main contribution of this paper is two-fold. First, the presentation of damping controller that uses a notch filter to damp the first resonant mode and a high-pass resonant controller to increase the bandwidth. Second, the propose of the hybrid model-based RMM and data-driven VRFT approach for parameters' optimization of the fixed order damping controller.

The remainder of this paper is organized as follows. In Section 2, the experimental setup used in the present study is described. The design of the paralleled controller that consists of a high-gain notch filter and a high-pass resonant controller using the proposed hybrid approach is presented in Section 3. Section 4 discusses the experimental verification of the designed controller. Finally, the paper is concluded in Section 5.

2. Experimental Setup and System Identification

2.1 Experimental setup

The controller designed is implemented on a three axis piezoelectric stack-actuated nanopositioning stage (P-561.3CD, Physik Instrumente) as shown in Fig. 1.

The terminal motion produced by the actuator is within 0-100 μm for each individual axis. The control input voltage (0-10 V) for each axis is produced by 18-bit digital to analog converters (DACs) of the data acquisition card (PCI 6281, National Instrument) and subsequently

amplified via a piezo amplifier module (E-503.00, Physik Instrumente) with a fixed gain of 10 to provide excitation voltage (0-100 V). The displacement of the output is read via a sensor monitor (E-509.C3A, Physik Instrumente) and is passed to the data acquisition card (PCI 6281, National Instrument) equipped with 18-bit analog to digital converters (ADCs).

The nanopositioning stage is controlled by Simulink Real-Time (Mathworks). The control algorithm is designed in Matlab/Simulink block diagram on the host PC, and then downloaded and executed in real-time on the target PC (CPU: Intel Core i5 @3.3 GHz).

In this work, only the X direction was used to implement the propose controller for damping SISO systems and the sampling frequency of the system was set to 10 kHz.

2.2 System identification

The transfer function of the X-axis can be described as

$$G(s)=\frac{D(s)}{V(s)} \tag{1}$$

where $D(s)$ is the Laplace transform of the output voltage collected from X sensor and $V(s)$ is the corresponding Laplace transform of the input voltage applied into X piezo. To obtain the corresponding actual displacement of the axes, a multiplication between a calibration factor of 10 μm/V and the sensor output voltage needs to be operated.

A linear model of the X-axis was obtained by applying a step voltage at 1 V into the electrode and recording the corresponding sensor output through the data acquisition card. Then, the system identification toolbox in MATLAB was used to identify the dynamic model. The obtained continuous transfer function is displayed in Eq. (2). Fig. 2 depicts the match between the measured and the identified open-loop step response of the X-axis dynamics. The step response of the identified model has a 99.903% fit with the measured results. In the determination of the parameters in the denominator of the controller, this model will be used in the RMM approach. The bode plot of $G(s)$ is shown in Fig. 3. The first resonant mode occurs at the frequency of 211 Hz, where the damping controller is to be designed to reject the unexpected vibrations.

$$G(s)=\frac{\begin{array}{l}-1.64\times10^{4}s^{6}+7.64\times10^{7}s^{5}+4.62\times10^{11}s^{4}\\+1.11\times10^{14}s^{3}+4.54\times10^{17}s^{2}+7.61\times10^{18}s\\+8.69\times10^{18}\end{array}}{\begin{array}{l}s^{8}+1.81\times10^{3}s^{7}+3.85\times10^{6}s^{6}+4.46\times10^{9}s^{5}\\+3.86\times10^{12}s^{4}+2.24\times10^{15}s^{3}+5.89\times10^{17}s^{2}\\+9.15\times10^{18}s+1.02\times10^{19}\end{array}} \tag{2}$$

3. Damping Controller Design

In this section, the hybrid RMM and VRFT approach is proposed first. Then, a high-gain notch filter is designed to damp the first resonant mode as shown in Fig. 3. Besides, the hysteresis and creep of the piezo actuator can be minimized through the high-gain control. A paralleled high-pass resonant controller is added to increase the closed-loop bandwidth as depicted in Fig. 7. In the design process, the RMM approach is applied to compute the parameters in the denominators of the two paralleled controllers, while the VRFT approach is adopted to calculate the parameters in the numerators. The overall design utilizes a hybrid model-based and data-driven approach to achieve an optimal damping controller for the nanopositioner in Fig. 1.

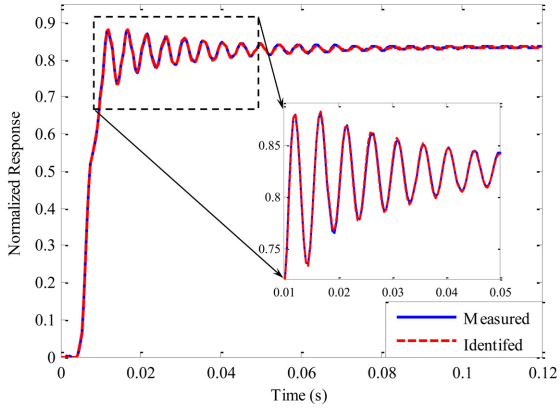

Fig. 2 The measured and the identified model step response of $G(s)$

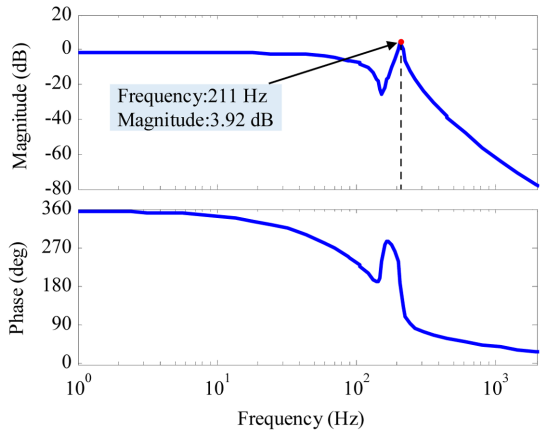

Fig. 3 Bode plot of the open-loop system $G(s)$

3.1 The hybrid RMM and VRFT approach

A brief review of the RMM and the VRFT approaches is given here, and the hybrid design approach is proposed before controller design.

3.1.1 Reference model matching (RMM)

The RMM approach is based on the identified system model and norm optimization operation.[13] The desired closed-loop transfer function should be chosen according to the design aim. Then, the optimization operation of minimizing the performance index $J_{MR}(\rho)$ needs to be conducted as

$$J_{MR}(\rho)=\left\|T(s)-\frac{G(s)C(s;\rho)}{1+G(s)C(s;\rho)}\right\| \tag{3}$$

where ρ donotes the parameters in the controller, $T(s)$ is the desired closed-loop transfer function, $G(s)$ is the plant transfer function, and $C(s;\rho)$ represents controller transfer function.[40]

3.1.2 Virtual reference feedback tuning (VRFT)

The VRFT approach is non-iterative feedback tuning. An input data $u(t)$ and the corresponding experimental output data $y(t)$ are collected through either an open-loop or a closed-loop experiment. The virtual reference signal $\bar{r}(t)$ then can be calculated as

$$T(s)\bar{r}(t) = y(t)\,. \tag{4}$$

The controller parameters can be calculated by minimize the following criterion as

$$J_{VR}(\rho) = \frac{1}{N}\sum_{t=1}^{N}((L(s)u(t) - C(s;\,\rho))L(s)e(t))^2 \tag{5}$$

where $L(s)$ is a filter, $C(s;\,\rho) = \beta^T(s)\rho$ is the controller and β(s) is the parameter independent vector of transfer functions, $e(t) = \bar{r}(t) - y(t)$ is the corresponding error.[40] The optimized parameter vector is given by

$$\hat{\rho}_{VR} = \left[\sum_{t=1}^{N}\varphi_L(t)\varphi_L(t)^T\right]^{-1}\sum_{t=1}^{N}\varphi_L(t)u_L(t)^T \tag{6}$$

where $\varphi_L(t) = L(s)\beta(s)e(t)$ and $u_L(t) = L(s)u(t)$.

3.1.3 The hybrid approach

Both the above-mentioned two approaches have limitations in controller design practice. When applying the RMM approach, choosing the initial values of the controller parameters is vital to ensure the convergence of the optimization process.[13] If the chosen initial values are not in a proper neighborhood of the optimal values, the optimization process will not obtain the optimal values. With respect to the VRFT approach, as can be seen in Eq. (5), the controller needs to be reorganized as the product of a parameter vector and a parameter independent vector of transfer functions. This leads to the limitation that there should be no parameters in the denominator of the controller.

For the optimization of the damping controller in this paper, the hybrid approach is proposed that will apply the RMM approach to determine the parameters in the denominator of the controller transfer function and use the VRFT approach to calculate the optimal parameters in the numerator. The performance index $J_H(\rho)$ is given as

$$J_H(\rho) = \left\| T(s) - \frac{G(s)\dfrac{N(s;\,\rho_{VR})}{D(s;\,\rho_{MR})}}{1 + G(s)\dfrac{N(s;\,\rho_{VR})}{D(s;\,\rho_{MR})}} \right\|_2^2 \tag{7}$$

where $\rho = [\rho_{VR}\ \rho_{MR}]$ is the parameter vector, $D(s;\,\rho_{MR})$ denotes the denominator of the controller obtained by the RMM approach, while $N(s;\,\rho_{MR})$ denotes the numerator of the controller obtained by the VRFT approach.

The optimization is an iterative process shown in Fig. 4, which can be described by steps as,

1. Choose the initial values of the parameters in the denominator ρ_{MR}^0 (The superscript *0* stands for the initial values) of the controller.
2. Calculate the corresponding parameters in the numerator ρ_{VR}^0 using VRFT approach.
3. Calculate the performance index $J_H(\rho)$ and updating the values of ρ_{MR}^i (i stands for the iteration index) in the direction of minimizing the performance index $J_H(\rho)$.

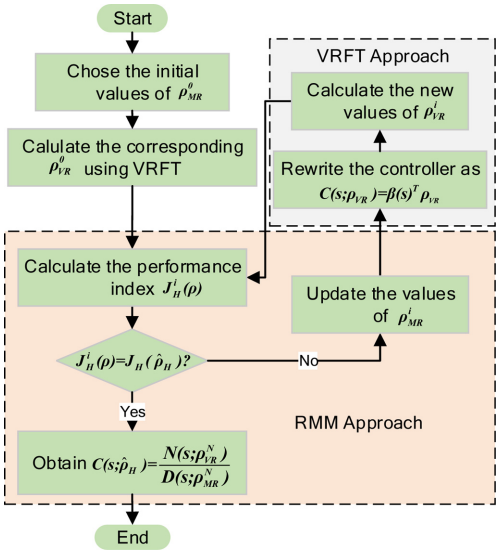

Fig. 4 The hybrid RMM and VRFT process

4. Calculate the corresponding parameters in the numerator ρ_{VR}^i using VRFT approach.
5. Repeat Step 3 and 4 to obtain a local minimizer of $J_H(\rho)$ and the optimal parameter vector $\hat{\rho}_H = [\rho_{VR}^N\ \ \rho_{MR}^N]$ (N stands for the convergent iteration).

The process of minimizing the performance index $J_H(\rho)$ can be implemented using the *fminsearch* command based on Nelder-Mead simplex algorithm[41] from the MATLAB. The initial values of ρ_H is set as $\rho_H^0 = [\rho_{VR}^0\ \ \rho_{MR}^0]$. The VRFT approach is added into the function handle of *fminsearch* command to update the values of ρ_{VR}^i corresponding to the optimized set of ρ_{MR}^i in each iteration.

The iterative process is a hybrid model-based and data-driven approach that takes the advantages of both the two approaches. The identified model is used to calculate the 2-norm of the error transfer function, while the VRFT approach uses a set of experimental data to calculate the parameters in the numerator of the controller to obtain an optimal controller when connecting with the actual system.

3.2 High-gain notch filter design

3.2.1 Design of notch filter

A notch filer is designed to modify the sharp resonant peak of the stage as described in Fig. 3. The notch filter was chosen as

$$C(s) = k_C\frac{s^2 + 2\xi_n\omega_n s + \omega_n^2}{s^2 + 2\xi_d\omega_d s + \omega_d^2} \tag{8}$$

where k_C is the static gain of the notch filter $C(s)$, ξ_n and ξ_d denote the damping constants of the second-order transfer function in the denominator and the numerator of the notch filter, ω_n and ω_d are the natural frequencies.

In the design of notch filter, the numerator was chosen to suppress the effect of the first resonant peak of the plant (at 211 Hz). To ensure that the filter was proper, the denominator was added at high frequencies to attenuate noise.[34] An integral item was added into the feedback notch filter to minimize the hysteresis and creep of the piezoelectric actuator as shown in Fig. 5.

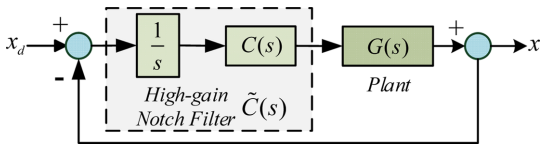

Fig. 5 The block diagram of the X-axis control system with high-gain notch filter

The hybrid approach was used in the controller design. First, from Eq. (2), the bandwidth of the open-loop system was identified as 43.7 Hz (The cross frequency at -3 dB in the bode plot). The desired closed-loop of the composite system with notch filter was chosen as

$$T(s) = \frac{2\pi f_0}{s + 2\pi f_0} \tag{9}$$

where f_0 is the desired bandwidth. Herein, the parameter f_0 was set 45 Hz according to the identified system in Eq. (2) and Fig. 3. The initial values of the parameters in the denominator were set as

$$\rho_{MR}^0 = [\xi_d^0 \quad \omega_d^0]^T = [0.5 \quad 3.142 \times 10^3 \text{ rad/s}]^T. \tag{10}$$

Then, the notch filter in Eq. (8) can be written more compactly in vector form as

$$\tilde{C}(s;\rho) = \beta(s)^T \rho_{VR} = \frac{1}{D(s;\rho_{MR}^0)\cdot s}[s^2 \quad s \quad 1]\begin{bmatrix} k_{C1} \\ k_{C2} \\ k_{C3} \end{bmatrix} \tag{11}$$

where the parameters $k_{C1} = k_c$, $k_{C2} = 2k_c\xi_n\omega_n$, $k_{C3} = k_c\omega_n^2$, and $D(s;\rho_{MR}^0) = s^2 + 2\xi_d^0\omega_d^0 s + (\omega_d^0)^2$. In order to compute the parameters using the VRFT approach, the filter was chosen as $L(s) = (1-T(s))T(s)\cdot\Phi_u^{-1}$ (Φ_u is the spectral density of input data $u(t)$).[40] A set of output data $y(t)$ was obtained by feeding the plant in open-loop with $N = 1024$ samples of a zero-mean Guassian white noise input data $u(t)$ ($\Phi_u = 0.1\ V$). Hereto, the parameters k_{C1}, k_{C2} and k_{C3} can be calculated through Eq. (6).

Last, an iterative optimizing process of the five parameters was implemented as described in section 3.1.3. The parameters was denoted in vector as $\rho_H = [\rho_{VR}; \rho_{MR}] = [k_c \ \xi_n \ \omega_n \ \xi_d \ \omega_d]^T$. The optimized parameter vector and the corresponding performance index are

$$\hat{\rho}_H = \begin{bmatrix} 3.766\times10^2 \\ 4.281 \\ 2.215\times10^4 \text{ rad/s} \\ 0.202 \\ 1.998\times10^3 \text{ rad/s} \end{bmatrix}, \quad J_H(\rho_H) = 0.59. \tag{12}$$

3.2.2 Performance of the notch filter

The performance of the composite system with the designed notch filter can be analyzed in both time and frequency domain as displayed in Figs. 6 and 7.

Fig. 6 shows the step response of the X-axis with and without the control of the notch filer. It can be seen that the composite system is stable and convergent. An improvement of 70 ms was achieved on the settling time from open-loop (102 ms) to closed-loop systems (32 ms). The stable error was decreased by 16.72% with notch filter.

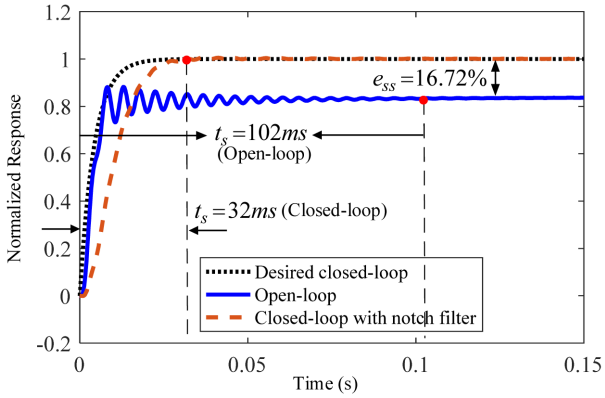

Fig. 6 Step response of the X-axis control system with and without notch filter

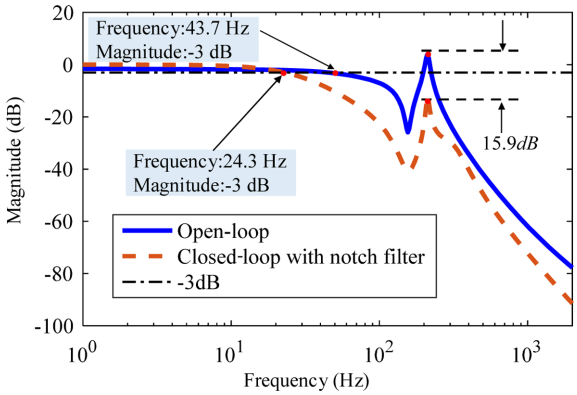

Fig. 7 Bode plots of the X-axis control system with and without notch filter

The bode plots of the X-axis with and without notch filter control are presented in Fig. 7. The designed notch filter modified the first resonant peak of the plant by a decrease of 15.9 dB (from 3.92 dB of the open-loop system to -12 dB of the closed-loop system). However, the bandwidth of the composite system was shrunk from 43.7 Hz to 24.3 Hz, which limited the accuracy of high-speed scanning of the nanopositioner. Therefore, a high-pass resonant controller needed to be added to increase the bandwidth of the composite system while not to raise up the first resonant peak.

3.3 High-pass resonant controller design

The composite control system of paralleled high-gain notch filter and high-pass resonant controller is depicted in Fig. 8. The resonant controller is a fixed-structure and low-order high-pass filter that can be optimized using the hybrid approach proposed in this paper. Herein, the composite controller for damping control proposed in this paper was doted as $C_{composite}(s;\rho) = \tilde{C}(s;\rho) + R(s;\rho)$.

3.3.1 Design of the composite controller

The transfer function of the resonant controller is chosen as

$$R(s) = \frac{k_{R1}s^2 + k_{R2}s}{s^2 + 2\xi_r\omega_r s + \omega_r^2} \tag{13}$$

where k_{R1} and k_{R2} are the gains in the numerator, ξ_r and ω_r denote the damping constant and the natural frequency of the resonant controller.

The parameters in $\tilde{C}(s)$ and $R(s)$ were optimized together through the proposed hybrid approach. Analogous to the design of notch filter, the desired closed-loop transfer function was chosen as Eq. (9), and a set of input and output data were obtained as described in section 3.2. The initial values of the parameters in the denominator of the composite controller were set as

$$\rho_{MR}^0 = \begin{bmatrix} \xi_d^0 \\ \omega_d^0 \\ \xi_r^0 \\ \omega_r^0 \end{bmatrix} = \begin{bmatrix} 0.5 \\ 3.142\times10^3 \text{ rad/s} \\ 0.1 \\ 2.512\times10^2 \text{ rad/s} \end{bmatrix} \tag{14}$$

where ω_d^0 was determined to attenuate noise at 500 Hz (equals to 3.142×10^3 rad/s), and ω_d^0 was chosen at 40 Hz (equals to 2.512×10^2 rad/s) to increase the closed-loop bandwidth.

Then, the composite controller in Fig. 7 was rewritten in vector form as

$$C_{composite}(s;\rho) = \beta(s)^T \rho_{VR} = \begin{bmatrix} \frac{s^2}{D_C(s;\rho_{MR}^0)\cdot s} \\ \frac{s}{D_C(s;\rho_{MR}^0)\cdot s} \\ \frac{1}{D_C(s;\rho_{MR}^0)\cdot s} \\ \frac{s^2}{D_R(s;\rho_{MR}^0)} \\ \frac{s}{D_R(s;\rho_{MR}^0)} \end{bmatrix}^T \begin{bmatrix} k_{C1} \\ k_{C2} \\ k_{C3} \\ k_{R1} \\ k_{R2} \end{bmatrix} \tag{15}$$

where the parameters were $k_{C1} = k_c$, $k_{C2} = 2k_c\xi_n\omega_n$, $k_{C3} = k_c\omega_n^2$, and the denominators of the controller were denoted as $D_C(s;\rho_{MR}^0) = s^2 + 2\xi_d^0\omega_d^0 s + (\omega_d^0)^2$, $D_R(s;\rho_{MR}^0) = s^2 + 2\xi_r^0\omega_r^0 s + (\omega_r^0)^2$.

The parameters in the composite controller was denoted as $\rho_H = [\rho_C, \rho_R]^T = [k_C\ \xi_n\ \omega_n\ \xi_d\ \omega_d,\ k_{R1}\ k_{R2}\ \xi_r\ \omega_r]^T$, where ρ_C and ρ_R were the parameters in notch filter and the resonant controller, respectively. The optimized parameter vector and the corresponding performance index through an iterative optimizing process were obtained as

$$\hat{\rho}_C = \begin{bmatrix} 2.231\times10^2 \\ -10.286 \\ 2.340\times10^4 \text{ rad/s} \\ 0.198 \\ 2.011\times10^3 \text{ rad/s} \end{bmatrix}, \quad \hat{\rho}_R = \begin{bmatrix} 0.245 \\ 2.065 \text{ rad/s} \\ 0.061 \\ 3.014\times10^2 \text{ rad/s} \end{bmatrix}, \tag{16}$$

$$J_H(\rho_H) = J_H([\rho_C, \rho_R]) = 0.66\,. \tag{17}$$

3.3.2 Performance of the composite controller

The bode plot of the composite control system with the designed notch filter paralleled with resonant controller is displayed in Fig. 9. By adding a paralleled resonant controller, the first resonant peak was damped by 18.4 dB which was better than that under mere notch filer controller (15.9 dB). On the other hand, the bandwidth of the closed-loop system was increased to 42.9 Hz (near the 43.7 Hz of open-loop bandwidth) under the composite control, which was markedly better than that under notch filter control (24.3 Hz). Therefore, the aim of damping the first resonant peak and maintaining the system bandwidth was achieved under the proposed composite controller designed by the hybrid approach.

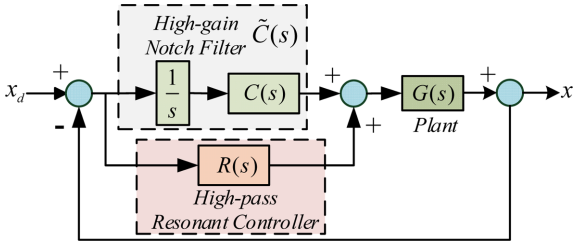

Fig. 8 The block diagram of the X-axis control system with paralleled high-gain notch filter and high-pass resonant controller

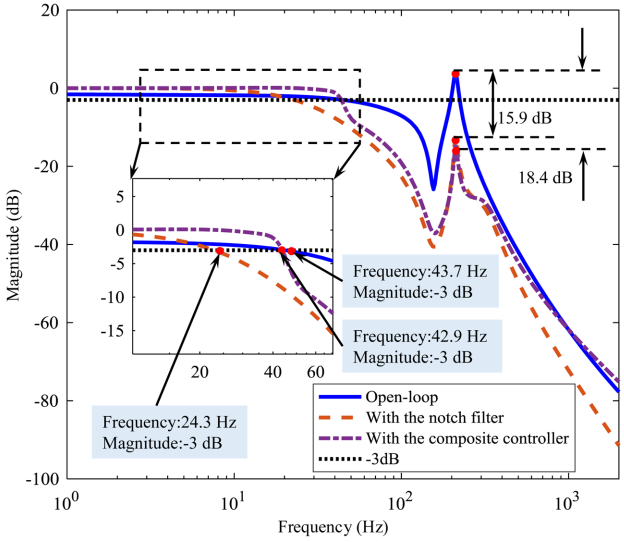

Fig. 9 Bode plots of the composite control system

3.4 The overall design procedure

3.4.1 Damping controller design using the hybrid approach

The paralleled high-gain notch filter and high-pass resonant controller designed using the proposed hybrid RMM and VRFT approach in this paper can be summarized as following steps:

1. Chose the desired closed-loop transfer function as Eq. (9).
2. Determine the initial values in the denominators of the controllers as Eq. (14).
3. Rewrite the controller in vector form as Eq. (15).
4. Compute the initial values of the parameters in the numerators of the controllers as described in Section 3.1.2.
5. Optimize the performance index in Eq. (7) through an iterative process (Section 3.1.3) to obtain the final set of parameters in the denominators of the controller. In each iteration, the parameters in the numerators can be calculated through VRFT approach. Finally, a set of the complete parameters in the composite damping controller can be obtained as shown in Eq. (16).

3.4.2 Comparison with RMM

The advantages of the proposed hybrid RMM and VRFT approach over the RMM approach alone for the damping controller design is two-fold.

Frist, there are nine parameters in the composite damping controller. When designing using the RMM approach alone, the initial values of the whole nine parameters need to be determined in proper intervals for searching for the optimal local values. While, when using the proposed hybrid approach, only four parameters in the denominator need to be chosen the initial values. Moreover, the four parameters in the denominator are less important than the five parameters in the numerator with respect to the static gain of the designed closed-loop system.

Second, the hybrid RMM and VRFT approach use the experimental data of the open-loop plant, which is advantageous on suppressing the model uncertainty compared with the RMM approach alone.

4. Experimental Verification

The designed composite controller using the hybrid approach was verified experimentally in the setup described in Fig. 1. Results of compensation for creep and hysteresis through high-gain feedback in the composite controller are presented in Section 4.1. Results of triangular trajectory tracking at 5 Hz, 10 Hz, and 25 Hz are presented in Section 4.2 to demonstrate the effectiveness of the composite damping control.

4.1 Creep and hysteresis control

Experimental results of the creep compensation are depicted in Fig. 10. For open-loop system, it took 7.5 minutes to rise from the initial value to the desired stable value, and the maximum error reached 0.922 μm (9.22% of the desired step). Under the control of the designed composite controller, the creep errors were obviously compensated, with a maximum error of 0.04 μm (0.4% of the desired step).

Fig. 11 displays the experimental results of the hysteresis compensation with and without the designed composite damping controller. Ten sets of back and forth trajectories with the minimum magnitude of 0.5 μm and the maximum magnitude of 10 μm (10% of the stroke of the stage) were fed to the input channel of the X-axis. Results demonstrated that the composite damping controller was effective on hysteresis compensation with a maximum error of 0.07 μm (0.7% of the maximum magnitude of 10 μm). For comparison, without the controller, the maximum error reached 0.73 μm.

4.2 Triangular trajectory tracking

As mentioned before, for image scanning of specimens, the nanopositioners are commonly actuated in a taster pattern with a triangular signal in the X-axis. To verify the effectiveness of the designed composite controller using the proposed hybrid method, three sets of triangular signals at 5 Hz, 10Hz and 25 Hz were applied in the tracking experiments. Results of the performance under built-in PID control are also presented for comparisons with the designed notch filter and the composite controller.

The overall tracking results under the three sets of controllers are shown in the left column in Fig. 12. It can be seen that all the three feedback controllers result in tracking delay. However, for AFM imaging,

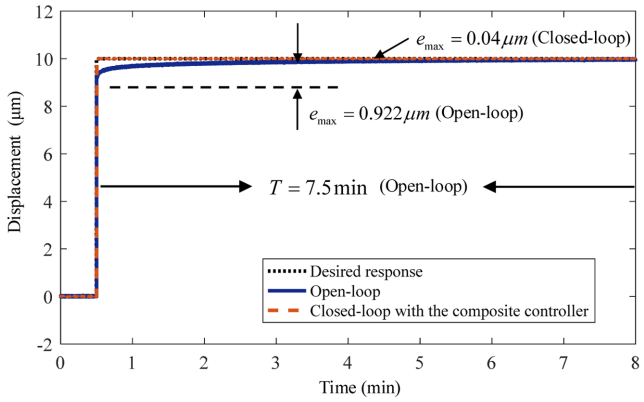

Fig. 10 Experimental results of creep compensation using the composite controller

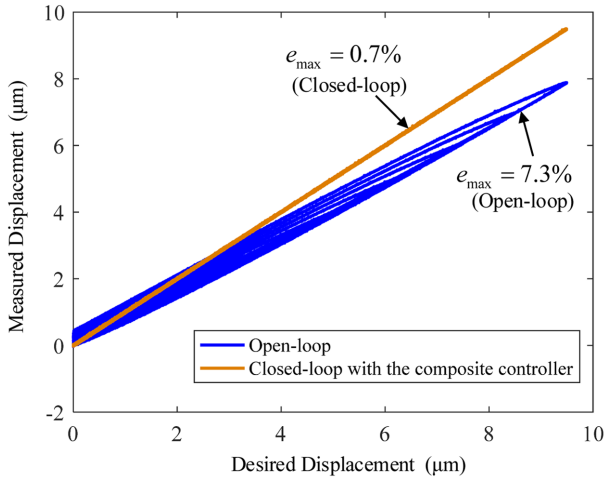

Fig. 11 Experimental results of hysteresis compensation using the composite controller

if the delay is known well, perfect delayed tracking is better than imperfect timely tracking.[42] So, to compare the performance under the three controllers, the delay is identified and removed before quantitative analysis. For detailed descriptions about the processing of the delay, readers can refer to Eq. (2) in the literature.[42] Shifted results of the overall tracking are presented in the right column in Fig. 12. The tracking errors after shifting are displayed in Fig. 13. It is obvious that both the alone notch filter controller and the composite controller achieved better tacking performance than the built-in PID.

To analyze the results qualitatively, the root mean squared (RMS) errors are calculated as shown in Table 1. It can be seen that performance under control of the notch filter alone is best, while the built-in PID achieves the worst performance. However, for AFM imaging, RMS errors might not tell the best measurements of tracking quality. As marked using the red dotted line in the three subplots in Fig. 13, tracking performance of the sharp corners of the triangular trajectory affects the final imaging quality. The maximum (MAX) tracking errors in the sharp corners at 5, 10 and 25 Hz under the three controllers are depicted in Table 2. It can be learned that with the increase of frequency, the composite controller worked better than the mere notch filter at sharp

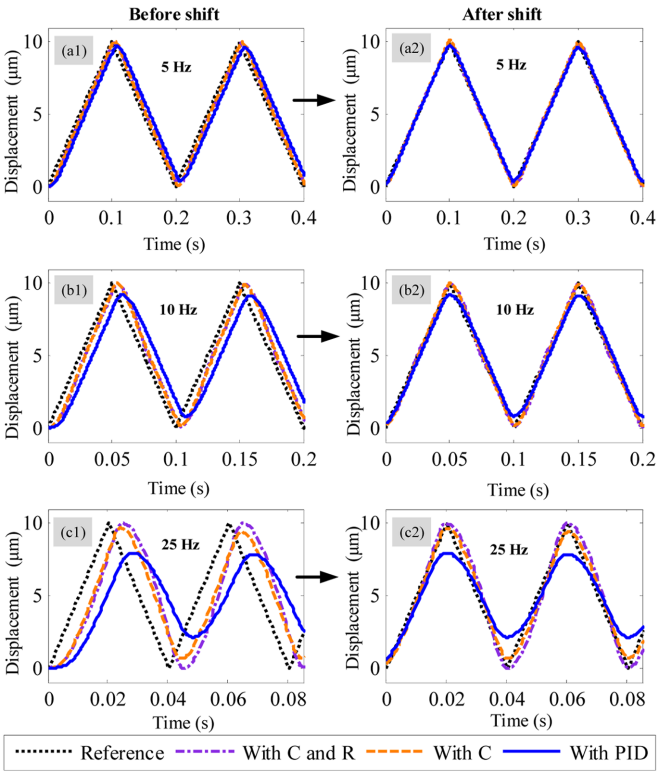

Fig. 12 Experimental results of the overall triangular trajectory tracking at (a) 5 Hz, (b) 10 Hz and (c) 25 Hz

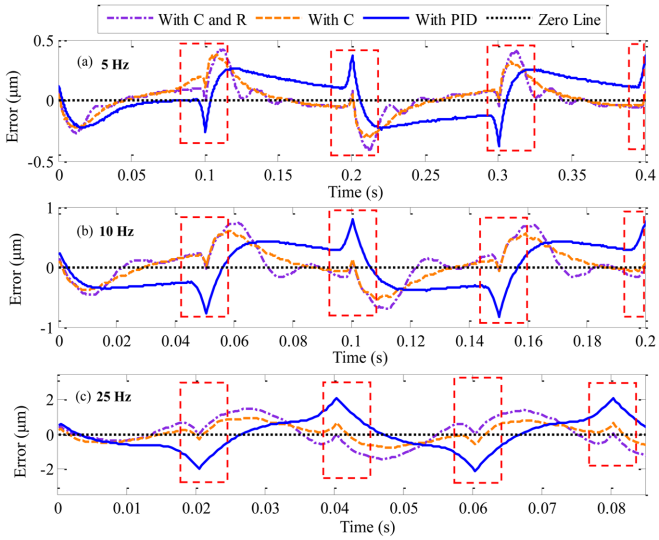

Fig. 13 Experimental results of triangular trajectory tracking errors at (a) 5 Hz, (b) 10 Hz and (c) 25 Hz

corners of the triangular trajectories. Similar to the results of RMS errors, the built-in PID controller results in the biggest MAX errors at the sharp corners.

5. Conclusions

In this study, a composite damping controller using a high-gain notch filter and a high-pass resonant controller was applied for vibration rejection of piezo-actuated nanopositioners. The hybrid reference model matching and virtual reference feedback tuning approach was proposed for parameters' optimization of the composite controller. In the stage of choosing the initial values, the number of the parameters was decreased to 4 from 9 for the presented damping controller using the hybrid RMM and VRFT approach. Besides, the experimental data was used to parameters' optimization to reject model uncertainty. A set of optimized parameters in the controller was obtained using the hybrid approach. Experimental results demonstrated that the proposed damping controller designed by the hybrid approach was effective on creep as well as hysteresis compensation and vibration rejection in triangular trajectory tracking cases.

Future works will seek to add proper feedforward controllers to eliminate the phase delay caused by the feedback damping controller as well as the parameters' optimization of the combined feedback and feedforward control system using data-driven approaches.

Table 1 RMS error values for triangular trajectory tracking

Controller	RMS Value (μm)		
	5 Hz	10 Hz	25 Hz
C	0.1351	0.2642	0.5001
C+R	0.1352	0.3101	0.8242
PID	0.1679	0.3623	0.9235

Table 2 MAX error values at sharp corners for triangular trajectory tracking

Controller	MAX Values at Sharp Corners (μm)		
	5 Hz	10 Hz	25 Hz
C	0.1051	0.1331	0.6543
C+R	0.0516	0.1038	0.1153
PID	0.3748	0.8295	2.1330

ACKNOWLEDGEMENT

This work was supported by the Natural Science Foundation of China under Grant 51375349 and Shenzhen Science and Technology Program under Grant JCYJ20170306171514468.

REFERENCES

1. Yong, Y., Moheimani, S. R., Kenton, B. J., and Leang, K., "High-Speed Flexure-Guided Nanopositioning: Mechanical Design and Control Issues," Review of scientific instruments, Vol. 83, No. 12, Paper No. 121101, 2012.

2. Hansen, H. N., Carneiro, K., Haitjema, H., and De Chiffre, L., "Dimensional Micro and Nano Metrology," CIRP Annals-Manufacturing Technology, Vol. 55, No. 2, pp. 721-743, 2006.

3. Eleftheriou, E., Antonakopoulos, T., Binnig, G., Cherubini, G., Despont, M., et al., "Millipede-A Mems-Based Scanning-Probe Data-Storage System," IEEE Transactions on Magnetics, Vol. 39,

No. 2, pp. 938-945, 2003.

4. Choi, K.-B. and Lee, J. J., "Passive Compliant Wafer Stage for Single-Step Nano-Imprint Lithography," Review of Scientific Instruments, Vol. 76, No. 7, Paper No. 075106, 2005.
5. Kang, D. and Gweon, D., "Development of Flexure Based 6-Degrees of Freedom Parallel Nano-Positioning System with Large Displacement," Review of Scientific Instruments, Vol. 83, No. 3, Paper No. 035003, 2012.
6. Zareinejad, M., Ghidary, S. S., Rezaei, S. M., and Abdullah, A., "Precision Control of a Piezo-Actuated Micro Telemanipulation System," Int. J. Precis. Eng. Manuf., Vol. 11, No. 1, pp. 55-65, 2010.
7. Schitter, G. and Rost, M. J., "Scanning Probe Microscopy at Video-Rate," Materials Today, Vol. 11, pp. 40-48, 2008.
8. Zou, Q., Leang, K. K., Sadoun, E., Reed, M., and Devasia, S., "Control Issues in High-Speed AFM for Biological Applications: Collagen Imaging Example," Asian Journal of Control, Vol. 6, No. 2, pp. 164-178, 2004.
9. Wang, Z., Witthauer, A., Zou, Q., Kim, G.-Y., and Faidley, L., "Control of a Magnetostrictive-Actuator-Based Micromachining System for Optimal High-Speed Microforming Process," IEEE/ASME Transactions on Mechatronics, Vol. 20, No. 3, pp. 1046-1055, 2015.
10. Eielsen, A. A., Vagia, M., Gravdahl, J. T., and Pettersen, K. Y., "Damping and Tracking Control Schemes for Nanopositioning," IEEE/ASME Transactions on Mechatronics, Vol. 19, No. 2, pp. 432-444, 2014.
11. Das, S. K., Pota, H. R., and Petersen, I. R., "A Mimo Double Resonant Controller Design for Nanopositioners," IEEE Transactions on Nanotechnology, Vol. 14, No. 2, pp. 224-237, 2015.
12. Das, S. K., Pota, H. R., and Petersen, I. R., "Damping Controller Design for Nanopositioners: A Mixed Passivity, Negative-Imaginary, and Small-Gain Approach," IEEE/ASME Transactions on Mechatronics, Vol. 20, No. 1, pp. 416-426, 2015.
13. Das, S. K., Pota, H. R., and Petersen, I. R., "Multivariable Negative-Imaginary Controller Design for Damping and Cross Coupling Reduction of Nanopositioners: A Reference Model Matching Approach," IEEE/ASME Transactions on Mechatronics, Vol. 20, No. 6, pp. 3123-3134, 2015.
14. Shan, Y. and Leang, K. K., "Design and Control for High-Speed Nanopositioning: Serial-Kinematic Nanopositioners and Repetitive Control for Nanofabrication," IEEE Control Systems, Vol. 33, No. 6, pp. 86-105, 2013.
15. Huang, S.-C. and Dao, T.-P., "Design and Computational Optimization of a Flexure-Based XY Positioning Platform Using FEA-Based Response Surface Methodology," Int. J. Precis. Eng. Manuf., Vol. 17, No. 8, pp. 1035-1048, 2016.
16. Liu, P.-B., Yan, P., Zhang, Z., and Leng, T.-T., "Flexure-Hinges Guided Nano-Stage for Precision Manipulations: Design, Modeling and Control," Int. J. Precis. Eng. Manuf., Vol. 16, No. 11, pp. 2245-2254, 2015.
17. Li, Y., Xiao, S., Xi, L., and Wu, Z., "Design, Modeling, Control and Experiment for a 2-DOF Compliant Micro-Motion Stage," Int. J. Precis. Eng. Manuf., Vol. 15, No. 4, pp. 735-744, 2014.
18. Mahmood, I. A. and Moheimani, S. O. R., "Making a Commercial Atomic Force Microscope More Accurate and Faster Using Positive Position Feedback Control," Review of Scientific Instruments, Vol. 80, No. 6, Paper No. 063705, 2009.
19. Clayton, G. M., Tien, S., Leang, K. K., Zou, Q., and Devasia, S., "A Review of Feedforward Control Approaches in Nanopositioning for High-Speed SPM," Journal of Dynamic Systems, Measurement, and Control, Vol. 131, No. 6, Paper No. 061101, 2009.
20. Leang, K. K. and Devasia, S., "Design of Hysteresis-Compensating Iterative Learning Control for Piezo-Positioners: Application to Atomic Force Microscopes," Mechatronics, Vol. 16, No. 3, pp. 141-158, 2006.
21. Fleming, A. J. and Wills, A. G., "Optimal Periodic Trajectories for Band-Limited Systems," IEEE Transactions on Control Systems Technology, Vol. 17, No. 3, pp. 552-562, 2009.
22. Butterworth, J. A., Pao, L. Y., and Abramovitch, D. Y., "A Comparison of Control Architectures for Atomic Force Microscopes," Asian Journal of Control, Vol. 11, No. 2, pp. 175-181, 2009.
23. Salapaka, S., Sebastian, A., Cleveland, J. P., and Salapaka, M. V., "High Bandwidth Nano-Positioner: A Robust Control Approach," Review of Scientific Instruments, Vol. 73, No. 9, pp. 3232-3241, 2002.
24. Aphale, S. S., Ferreira, A., and Moheimani, S. R., "A Robust Loop-Shaping Approach to Fast and Accurate Nanopositioning," Sensors and Actuators A: Physical, Vol. 204, pp. 88-96, 2013.
25. Lee, C. and Salapaka, S. M., "Fast Robust Nanopositioning – A Linear-Matrix-Inequalities-Based Optimal Control Approach," IEEE/ASME Transactions on Mechatronics, Vol. 14, No. 4, pp. 414-422, 2009.
26. Ratnam, M., Bhikkaji, B., Fleming, A., and Moheimani, S., "PPF Control of a Piezoelectric Tube Scanner," Proc. of 44th IEEE Conference on Decision and Control Conference (CDC-ECC), pp. 1168-1173, 2005.
27. Aphale, S. S., Bhikkaji, B., and Moheimani, S. R., "Minimizing Scanning Errors in Piezoelectric Stack-Actuated Nanopositioning Platforms," IEEE Transactions on Nanotechnology, Vol. 7, No. 1, pp. 79-90, 2008.
28. Bhikkaji, B., Ratnam, M., Fleming, A. J., and Moheimani, S. O. R., "High-Performance Control of Piezoelectric Tube Scanners," IEEE Transactions on Control Systems Technology, Vol. 15, No. 5, pp. 853-866, 2007.
29. Fairbairn, M. and Moheimani, S., "Resonant Control of an Atomic Force Microscope Micro-Cantilever for Active Q Control," Review

of Scientific Instruments, Vol. 83, No. 8, Paper No. 083708, 2012.

30. Das, S. K., Pota, H. R., and Petersen, I. R., "Resonant Controller Design for a Piezoelectric Tube Scanner: A Mixed Negative-Imaginary and Small-Gain Approach," IEEE Transactions on Control Systems Technology, Vol. 22, No. 5, pp. 1899-1906, 2014.
31. Fleming, A. J., Aphale, S. S., and Moheimani, S. R., "A New Method for Robust Damping and Tracking Control of Scanning Probe Microscope Positioning Stages," IEEE Transactions on Nanotechnology, Vol. 9, No. 4, pp. 438-448, 2010.
32. Bhikkaji, B. and Moheimani, S. R., "Integral Resonant Control of a Piezoelectric Tube Actuator for Fast Nanoscale Positioning," IEEE/ASME Transactions on Mechatronics, Vol. 13, No. 5, pp. 530-537, 2008.
33. Namavar, M., Fleming, A. J., Aleyaasin, M., Nakkeeran, K., and Aphale, S. S., "An Analytical Approach to Integral Resonant Control of Second-Order Systems," IEEE/ASME Transactions on Mechatronics, Vol. 19, No. 2, pp. 651-659, 2014.
34. Leang, K. K. and Devasia, S., "Feedback-Linearized Inverse Feedforward for Creep, Hysteresis, and Vibration Compensation in AFM Piezoactuators," IEEE Transactions on Control Systems Technology, Vol. 15, No. 5, pp. 927-935, 2007.
35. Formentin, S., Heusden, K., and Karimi, A., "A Comparison of Model-Based and Data-Driven Controller Tuning," International Journal of Adaptive Control and Signal Processing, Vol. 28, No. 10, pp. 882-897, 2014.
36. Formentin, S., Savaresi, S., and Del Re, L., "Non-Iterative Direct Data-Driven Controller Tuning for Multivariable Systems: Theory and Application," IET Control Theory & Applications, Vol. 6, No. 9, pp. 1250-1257, 2012.
37. Wellstead, P. E., Edmunds, J. M., Prager, D., and Zanker, P., "Self-Tuning Pole/Zero Assignment Regulators," International Journal of Control, Vol. 30, No. 1, pp. 1-26, 1979.
38. Hjalmarsson, H., Gevers, M., Gunnarsson, S., and Lequin, O., "Iterative Feedback Tuning: Theory and Applications," IEEE Control Systems, Vol. 18, No. 4, pp. 26-41, 1998.
39. Karimi, A., Mišković, L., and Bonvin, D., "Iterative Correlation-Based Controller Tuning," International Journal of Adaptive Control And Signal Processing, Vol. 18, No. 8, pp. 645-664, 2004.
40. Campi, M. C., Lecchini, A., and Savaresi, S. M., "Virtual Reference Feedback Tuning: A Direct Method for the Design of Feedback Controllers," Automatica, Vol. 38, No. 8, pp. 1337-1346, 2002.
41. Lagarias, J. C., Reeds, J. A., Wright, M. H., and Wright, P. E., "Convergence Properties of the Nelder-Mead Simplex Method in Low Dimensions," SIAM Journal on Optimization, Vol. 9, No. 1, pp. 112-147, 1998.
42. Butterworth, J. A., Pao, L. Y., and Abramovitch, D. Y., "A Comparison of ILC Architectures for Nanopositioners with Applications to AFM Raster Tracking," Proc. of American Control Conference (ACC), pp. 2266-2271, 2011.